*Inorg. Chem.* **2002**, *41*, 4266–4274

# Competing Interactions in the Tetranuclear Spin Cluster $\{Ni[(OH)_2Cr(bispictn)]_3\}I_5 \cdot 5H_2O$. An Inelastic Neutron Scattering and Magnetic Study

**Ralph Schenker,[†,||] Høgni Weihe,[‡] Hanspeter Andres,[†] Reto Basler,[†] Grégory Chaboussant,[†] Kirsten Michelsen,[‡] Michael Aebersold,[†] Herma BUttner,[§] and Hans U. GUdel*[,†]**

*Departement für Chemie und Biochemie, Universität Bern, Freiestrasse 3, CH-3000 Bern 9, Switzerland, H. C. Ørsted Institutet, Københavns Universitet, Universitetsparken 5, DK-2100 København Ø, Denmark, and Institute Laue Langevin, Avenue des Martyrs, B. P. 156, F-38042 Grenoble, France*

Received October 23, 2001

The properties of the spin state manifold of the tetranuclear cluster $Ni[(OH)_2Cr(bispictn)]_3\}I_5 \cdot 5H_2O$ (bispictn = *N*,*N*′-bis(2-pyridylmethyl)-1,3-propanediamine) are investigated by combining magnetic susceptibility and magnetization measurements with an inelastic neutron scattering (INS) study on an undeuterated sample of $Ni[(OH)_2Cr(bispictn)]_3\}I_5 \cdot 5H_2O$. The temperature dependence of the magnetic susceptibility indicates an $S = {}^1/_2$ ground state, which requires antiferromagnetic interactions both between $Cr^{3+}$ and $Ni^{2+}$ ions and among the $Cr^{3+}$ ions. INS reveals potential single-ion anisotropies to be negligibly small and enables an accurate determination of the exchange parameters. The best fit to the experimental energy level diagram is obtained by an isotropic spin Hamiltonian $H = J_{CrNi}(\mathbf{S_1 \cdot S_4} + \mathbf{S_2 \cdot S_4} + \mathbf{S_3 \cdot S_4}) + J_{CrCr}(\mathbf{S_1 \cdot S_2} + \mathbf{S_1 \cdot S_3} + \mathbf{S_2 \cdot S_3})$ with $J_{CrNi} = 1.47$ cm$^{-1}$ and $J_{CrCr} = 1.25$ cm$^{-1}$. With this model, the experimental intensities of the observed INS transitions as well as the temperature dependence of the magnetic data are reproduced. The resulting overall antiferromagnetic exchange is rationalized in terms of orbital exchange pathways and compared to the situation in oxalato-bridged clusters.

## 1. Introduction

Compounds containing simple, isolated clusters of transition and rare earth metal ions with unpaired electrons serve as ideal molecular models to study exchange interactions. Complications arising from cooperative effects in systems with extended interactions are eliminated, allowing a detailed analysis of the nature and mechanisms of the exchange coupling. Therefore, exchange interactions in molecular dimer complexes have been studied extensively. However, heteronuclear dimers and clusters containing $Cr^{3+}$ and $Ni^{2+}$ ions are relatively unexplored. Magnetochemical studies on oxalato-,[1] dithiooxalato-,[2] and cyanide-bridged[3,4] tetranuclear clusters have been reported, in which the dominant exchange interaction between $Cr^{3+}$ and $Ni^{2+}$ ions is ferromagnetic, which was rationalized on the basis of the strict orthogonality of the $t_{2g}$ and $e_g$ magnetic orbitals on $Cr^{3+}$ and $Ni^{2+}$, respectively.[5] In corresponding compounds forming networks of oxalato-[6,7] and cyanide-bridged[8] $Cr^{3+}$ and $Ni^{2+}$ ions, this leads to ferromagnetic ordering. The design and construction of such molecule-based ferromagnets has become a very active area of research in recent years. In contrast, in oxo-[9,10] and hydroxo-bridged[11] complexes, antiferromagnetic interactions are dominant.

* To whom correspondence should be addressed. E-mail: guedel@iac.unibe.ch. Fax: +41 31 631 42 49.
† Universität Bern.
‡ Københavns Universitet.
§ Institute Laue Langevin.
|| Present address: Department of Chemistry, University of Wisconsin—Madison, 1101 University Avenue, Madison, WI 53706.

(1) Pei, Y.; Journaux, Y.; Kahn, O. *Inorg. Chem.* **1989**, *28*, 100.
(2) Mitsumi, M.; Okawa, H.; Sakiyama, H.; Ohba, M.; Matsumoto, N.; Kurisaki, T.; Wakita, H. *J. Chem. Soc., Dalton Trans.* **1993**, 2991.
(3) Mallah, T.; Auberger, C.; Verdaguer, M.; Veillet, P. *J. Chem. Soc., Chem. Commun.* **1995**, 61.
(4) Ohba, M.; Fukita, N.; Ôkawa, H. *J. Chem. Soc., Dalton Trans.* **1997**, 1733.
(5) Kahn, O. *Struct. Bonding (Berlin)* **1987**, *68*, 69.
(6) Tamaki, H.; Zhong, Z. J.; Matsumoto, N.; Kida, S.; Koikawa, M.; Achiva, N.; Hashimoto, Y.; Okawa, H. *J. Am. Chem. Soc.* **1992**, *114*, 6974.
(7) Coronado, E.; Galán-Mascarós, J. R.; Gómez-García, Martínez-Agudo, J. M. *Inorg. Chem.* **2001**, *40*, 113.
(8) Ferlay, S.; Mallah, T.; Vaissermann, J.; Bartolomé, F.; Veillet, P.; Verdaguer, M. *Chem. Commun.* **1996**, 2481 and references therein.



10.1021/ic0111031 CCC: $22.00 
Published on Web 07/20/2002

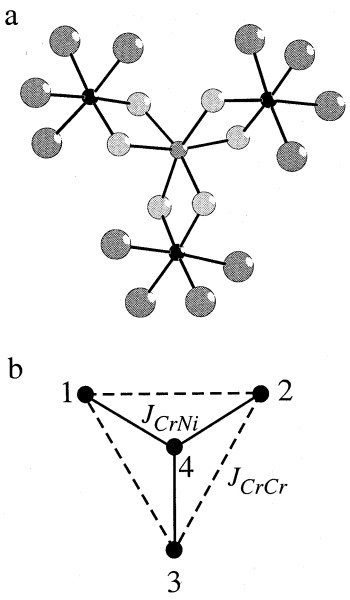


**Figure 1.** (a) Central core of the Ni[(OH)$_2$Cr(bispictn)]$_3$}X$_5$·5H$_2$O (X = I$^-$, ClO$_4^-$) (bispictn = *N*,*N*′-bis(2-pyridylmethyl)-1,3-propanediamine) cluster, abbreviated {Cr$_3$Ni}X$_5$, viewed along the pseudo-$C_3$ axis. The Cr$^{3+}$ ions are shown in black, and the central Ni$^{2+}$ ion and the nitrogen atoms, in darker gray, with larger spheres for the latter. The oxygen bridging atoms are shown in light gray. (b) Schematic representation of the exchange coupling in the {Cr$_3$Ni}$^{5+}$ clusters with the exchange parameters $J_{CrNi}$ and $J_{CrCr}$ denoting the Cr$^{3+}$−Ni$^{2+}$ and Cr$^{3+}$−Cr$^{3+}$ interactions, respectively.

Several years ago, the synthesis of {{Ni[(OH)$_2$Cr(bispictn)]$_3$}(ClO$_4$)$_5$·6H$_2$O (bispictn = *N*,*N*′-bis(2-pyridylmethyl)-1,3-propanediamine) (abbreviated {Cr$_3$Ni}(ClO$_4$)$_5$) was reported.[12] In this tetranuclear cluster, three Cr$^{3+}$ ions are each linked by two hydroxo bridges to the central Ni$^{2+}$ ion, forming a triangular core as depicted in Figure 1. On the basis of magnetic susceptibility data down to 5 K, both the Cr$^{3+}$−Ni$^{2+}$ and Cr$^{3+}$−Cr$^{3+}$ interactions were postulated to be antiferromagnetic with exchange parameter values of $J_{CrNi} = 4.87$ cm$^{-1}$ and $J_{CrCr} = 1.06$ cm$^{-1}$, respectively.[12] The resulting exchange splittings were found to be in the same order of magnitude as a potential zero-field splitting (ZFS) on the Ni$^{2+}$ ion. However, the two effects could not be unraveled on the basis of magnetic susceptibility data, and therefore, the anisotropy interaction was neglected in the analysis. We are here confronted with a typical problem of magnetic susceptibility measurements: This thermodynamic technique requires the construction of a microscopic model with a subsequent fit of the parameters to the experimental data. The danger in this procedure lies in the low information content of the susceptibility data, which often does not allow an unambiguous discrimination between physically different models. As will be shown in the present study, the {Cr$_3$Ni}$^{5+}$ cluster is an illustrative example in this respect. In our situation of competing interactions, magnetic measurements are clearly not sufficient to completely explore the ground state properties and thus unambiguously determine the nature of both the exchange and anisotropy interactions in this cluster.

Our approach to the energy splittings of the {Cr$_3$Ni}$^{5+}$ cluster is a more direct one. In addition to magnetic techniques, we use the complementary technique of inelastic neutron scattering (INS), which has proven to be extremely powerful to directly access the energies and eigenfunctions of the low-lying cluster spin states.[13] For safety reasons, we used {{Ni[(OH)$_2$Cr(bispictn)]$_3$}I$_5$·5H$_2$O (abbreviated {Cr$_3$Ni}I$_5$) instead of {Cr$_3$Ni}(ClO$_4$)$_5$ reported originally.[12,14] We find that both the net interactions between the Cr$^{3+}$ and Ni$^{2+}$ as well as among the Cr$^{3+}$ ions are antiferromagnetic, with comparable exchange parameter values. They are rationalized in terms of the orbital exchange pathways and compared with those in the oxalato-bridged clusters. Single-ion anisotropies are found to be negligibly small.

## 2. Experimental Section

**2.1. Synthesis.** All the chemicals used were at least of reagent grade and used without further purification.

***cis*-[Cr(bispictn)(H$_2$O)(OH)]I$_2$·2H$_2$O** was prepared as described previously.[12] Its purity was checked by X-ray powder diffraction using the structural data given in ref 15.

**{Ni[(OH)$_2$Cr(bispictn)]$_3$}I$_5$·5H$_2$O.** A 1.80 g (3 mmol) portion of *cis*-[Cr(bispictn)(H$_2$O)(OH)]I$_2$·2H$_2$O was suspended in H$_2$O (7.5 mL), 2 M NaOH (1.5 mL, 3 mmol) was added, and the solution was filtered into a beaker with 4 cm diameter. A 0.1 M NiCl$_2$ solution (10 mL, 1 mmol) was placed in a glass tube (15 mm diameter) sealed with a dialytical membrane at the lower end. At the same moment, the tube was dipped by 3 mm into the Cr$^{3+}$ solution. After several hours, polycrystalline aggregates started growing. After 3 days, they were filtered off and dried in air. The crystals crumbled upon drying. Yield: 60% of a red powder. Anal. Calcd for Cr$_3$NiC$_{45}$N$_{12}$H$_{76}$O$_{11}$I$_5$: Cr, 8.62%; Ni, 3.24%; C, 29.86%; N, 9.28%; H, 4.23%. Found: Cr, 8.70%; Ni, 3.18%; C, 29.85%; N, 8.50%; H, 4.24%.

The diffusion technique allowed us to obtain ill-shaped but transparent crystals of {Ni[(OH)$_2$Cr(bispictn)]$_3$}I$_5$·*x*H$_2$O ($x > 5$) up to 5 mm in size, which crumble to powder in air, indicating loss of solvent water. Elemental analysis and thermogravimetric measurements indicate that the resulting compound is {Ni[(OH)$_2$Cr(bispictn)]$_3$}I$_5$·5H$_2$O (abbreviated {Cr$_3$Ni}I$_5$). Except for slight line shifts, its X-ray powder diffractogram is essentially identical to that of {Ni[(OH)$_2$Cr(bispictn)]$_3$}I$_5$·*x*H$_2$O ($x > 5$) which, together with the results of the elemental analysis, indicates that {Cr$_3$Ni}I$_5$ consists of a single, pure phase. Examination of the intact crystals of {Ni[(OH)$_2$Cr(bispictn)]$_3$}I$_5$·*x*H$_2$O ($x > 5$) under a polarizing microscope revealed that they belong to one of the biaxial crystal systems and thus do not offer a crystallographically imposed trigonal site for the Ni$^{2+}$ ions. We can assume the same to be true for the crumbled product {Cr$_3$Ni}I$_5$. This is in contrast to {Cr$_3$Ni}(ClO$_4$)$_5$, for which both the crystal and cluster symmetries are exactly trigonal.[12]

(9) Blake, A. B.; Yavari, A.; Hatfield, W. E.; Sethulekshmi, C. N. *J. Chem. Soc., Dalton Trans.* **1985**, 2509.
(10) Blake, A. B.; Sinn, E.; Yavari, A.; Murray, K. S.; Moubaraki, B. *J. Chem. Soc., Dalton Trans.* **1998**, 45.
(11) Corbin, K. M.; Glerup, J.; Hodgson, D. J.; Lynn, M. H.; Michelsen, K.; Nielsen, K. M. *Inorg. Chem.* **1993**, *32*, 18.
(12) Hodgson, D. J.; Michelsen, K.; Pedersen, E.; Towle, D. K. *Inorg. Chem.* **1991**, *30*, 815.
(13) Güdel, H. U. In *Molecular Magnetism: From Molecular Assemblies to Devices*; Coronado, E., Delhas, P., Gatteschi, D., Miller, J. S., Eds.; NATO ASI Series E 321; Kluwer Academic Publishers: Dordrecht, The Netherlands, 1996; pp 229−242.
(14) INS experiments require sample amounts of several grams, a serious risk in view of the explosive character of perchlorates.
(15) Ardon, M.; Bino, A.; Michelsen, K.; Pedersen, E. *J. Am. Chem. Soc.* **1987**, *109*, 5855.

**{Zn[(OH)$_2$Cr(bispictn)]$_3$}I$_5$·5H$_2$O.** The preparation was analogous to that of {Ni[(OH)$_2$Cr(bispictn)]$_3$}I$_5$·5H$_2$O, using a 0.1 M solution of Zn(NO$_3$)$_2$·6H$_2$O. Yield: 45%. Anal. Calcd for $Cr_3ZnC_{45}N_{12}H_{76}O_{11}I_5$: Cr, 8.56%; Zn, 3.59%; C, 29.66%; N, 9.22%; H, 4.20%. Found: Cr, 8.85%; Ni, 3.98%; C, 30.08%; N, 9.17%; H, 4.23%.

The behavior of {Zn[(OH)$_2$Cr(bispictn)]$_3$}I$_5$·$x$H$_2$O ($x > 5$) upon drying was exactly analogous to the corresponding nickel complex, and the final product {Zn[(OH)$_2$Cr(bispictn)]$_3$}I$_5$·5H$_2$O (abbreviated {Cr$_3$Zn}I$_5$) was found to be isomorphous with {Cr$_3$Ni}I$_5$.

**2.2. Magnetic Measurements.** Variable temperature magnetic susceptibility measurements on polycrystalline samples of {Cr$_3$Ni}I$_5$ and {Cr$_3$Zn}I$_5$ were carried out in the temperature range 1.8−300 K at a magnetic field of 0.1 T using a Quantum Design MPMS-XL-5 magnetometer equipped with a SQUID (superconduction quantum interference device) sensor and a 5 T magnet. For magnetization measurements at higher magnetic fields up to 5 T, the sample was pressed to a pellet to avoid reorientation of the crystallites in the magnetic field. The data were corrected for the diamagnetic contributions of the atoms, which were estimated from Pascal's constants.

**2.3. Inelastic Neutron Scattering.** An amount of 7 g of a polycrystalline, completely undeuterated sample of {Cr$_3$Ni}I$_5$ was prepared and sealed under helium in an aluminum container of 15 mm diameter and 55 mm height suitable for INS experiments. These were performed with cold neutrons on the time-of-flight spectrometer IN5 at the Institut Laue Langevin (ILL) in Grenoble, France. Spectra were recorded at temperatures of 1.8, 7.0, and 17.0 K and with incident neutron wavelengths $\lambda$ of 4.2, 5.9, and 8.0 Å. The data treatment involved the subtraction of a background spectrum using an empty aluminum container of the same size and the calibration of the detectors with a spectrum of vanadium metal. The time-of-flight to energy conversion and the data reduction were done with the standard program INX at the ILL.

## 3. Results

**3.1. Magnetic Measurements.** The temperature dependences of the magnetic susceptibility of polycrystalline samples of {Cr$_3$Ni}I$_5$ and {Cr$_3$Zn}I$_5$ in the range 1.8−300 K are shown in the upper and lower panels of Figure 2, respectively, as plots of the product $\chi T$ versus $T$. For {Cr$_3$Ni}I$_5$, $\chi T$ slightly decreases from 6.58 cm$^3$ K mol$^{-1}$ at 300 K to a value of 6 cm$^3$ K mol$^{-1}$ at 60 K, before steeply dropping to 2.08 cm$^3$ K mol$^{-1}$ at 1.8 K. Similarly, for {Cr$_3$Zn}I$_5$, $\chi T$ decreases from 5.46 cm$^3$ K mol$^{-1}$ at 300 K to 1.48 cm$^3$ K mol$^{-1}$ at 1.8 K.

Figure 3 shows plots of the reduced magnetization $M/N\mu_B$ versus $H/T$ for {Cr$_3$Ni}I$_5$ between 1.8 and 40 K at various magnetic fields between 0.5 and 5 T as indicated. The magnetization curves are strongly field dependent. The magnetic moment per cluster in units of Bohr magnetons at 1.8 K is increasing with increasing magnetic field up to a value of 6 at 5 T and 1.8 K, where it is still not saturated.

**3.2. Inelastic Neutron Scattering.** In Figure 4, we show the INS spectra of a polycrystalline sample of {Cr$_3$Ni}I$_5$ with an incident neutron wavelength $\lambda$ of 8.0 Å at 1.8 and 7.0 K. The energy-transfer range between −5 and +5 cm$^{-1}$ is depicted with positive values for neutron-energy loss. The instrumental resolution is 0.22 cm$^{-1}$ at the elastic peak position. At 1.8 K, two prominent, nicely resolved peaks are observed at 1.65 and 2.21 cm$^{-1}$ on the neutron-energy loss side, labeled I and II, respectively. The corresponding energy-gain transitions, labeled I′ and II′, respectively, are observed as weak but distinct bands at this temperature. Increasing the temperature to 7.0 K results in a decrease of the scattering intensity of bands I and II and an increase of I′ and II′. There is a shoulder below 0.8 cm$^{-1}$, which does not show a

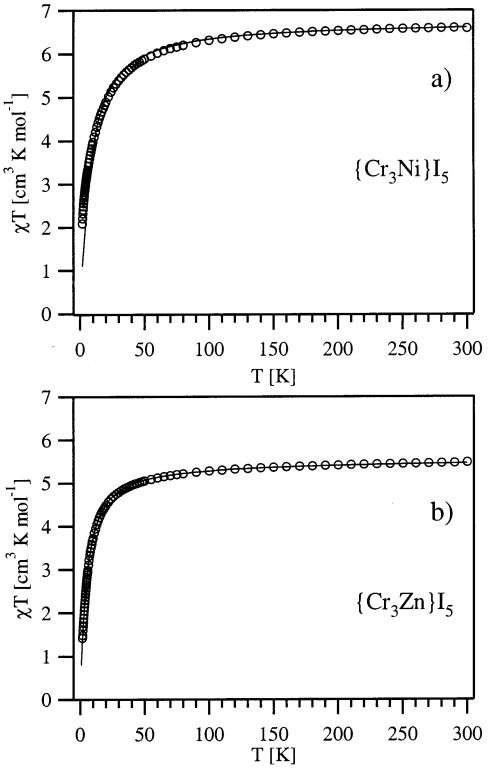


**Figure 2.** Temperature dependences of the molar magnetic susceptibility plotted as product $\chi T$ versus $T$ between 1.8 and 300 K. Experimental data for {Cr$_3$Ni}I$_5$ and {Cr$_3$Zn}I$_5$ are shown as open circles (○) in the upper and lower panels, respectively. The solid lines represent the best fits using the second term in eq 1 and the appropriate Zeeman term with the parameter values $J_{CrCr} = 1.12$ cm$^{-1}$ and $g_{Cr} = 1.97$ for {Cr$_3$Zn}I$_5$, as well as $g_{Cr} = 1.97$, $g_{Ni} = 2.26$ and the fixed parameters $J_{CrNi} = 1.47$ cm$^{-1}$, $J_{CrCr} = 1.25$ cm$^{-1}$ for {Cr$_3$Ni}I$_5$.

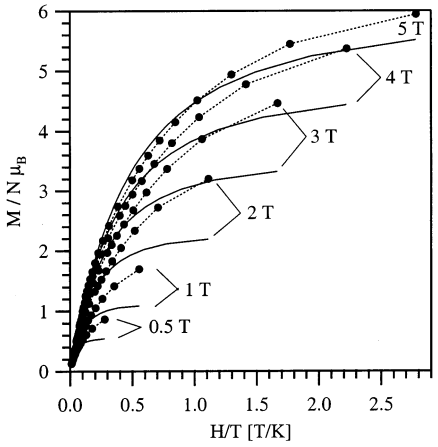


**Figure 3.** Plots of the reduced magnetization $M/N\mu_B$ versus $H/T$ for {Cr$_3$Ni}I$_5$ between 1.8 and 40 K. Data were collected at six magnetic fields between 0.5 and 5 T as indicated. The solid lines represent the calculated curves using eq 1 together with the appropriate Zeeman term using the parameter values $J_{CrNi} = 1.47$ cm$^{-1}$, $J_{CrCr} = 1.25$ cm$^{-1}$, $g_{Cr} = 1.97$, and $g_{Ni} = 2.26$.

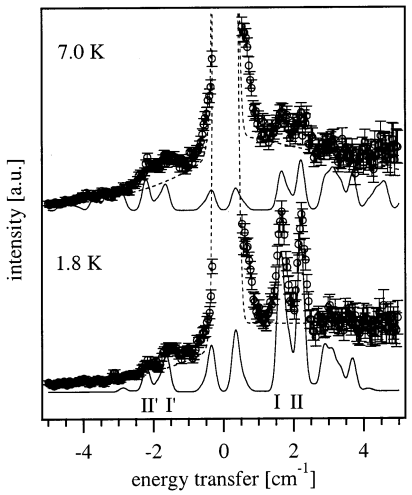


**Figure 4.** Neutron-energy loss and gain spectra of the polycrystalline sample {$Cr_3Ni$}$I_5$ measured on IN5 with an incident neutron wavelength of 8.0 Å at 1.8 and 7.0 K. The observed bands are labeled with Roman letters. The dashed lines represent a convolution of the experimental background and the elastic peak. The solid lines represent the calculated spectra using the program ANIMAG[21] with the parameter values $J_{CrNi} = 1.47$ cm$^{-1}$ and $J_{CrCr} = 1.25$ cm$^{-1}$.

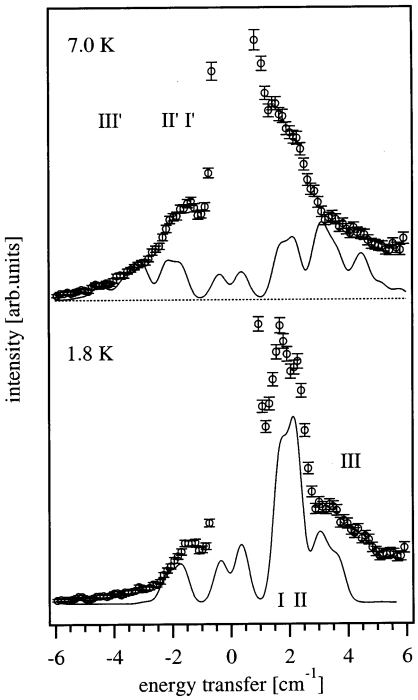


**Figure 5.** Neutron-energy loss and gain spectra of the polycrystalline sample {$Cr_3Ni$}$I_5$ measured on IN5 with an incident neutron wavelength of 5.9 Å at 1.8 and 7.0 K. The observed peaks are labeled with Roman letters. The solid lines represent the calculated spectra using the program ANIMAG[21] with the parameter values $J_{CrNi} = 1.47$ cm$^{-1}$ and $J_{CrCr} = 1.25$ cm$^{-1}$.

counterpart on the neutron energy gain side upon heating. Thus, it is at least partly due to an experimental artifact.

INS spectra with $\lambda = 5.9$ Å are shown in Figure 5 at 1.8 and 7.0 K. According to the decreased instrumental resolution of 0.54 cm$^{-1}$ at the elastic peak position compared to the 8.0 Å spectra, the bands I and II are only partly resolved. Furthermore, they seem to be superimposed by artificial features. An additional, broad band is observed centered at about 4 cm$^{-1}$, labeled III in Figure 5. It is essentially

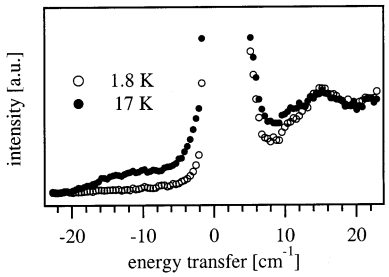


**Figure 6.** Neutron-energy loss and gain spectra of the polycrystalline sample {$Cr_3Ni$}$I_5$ measured on IN5 with an incident neutron wavelength of 4.2 Å at 1.8 and 17 K.

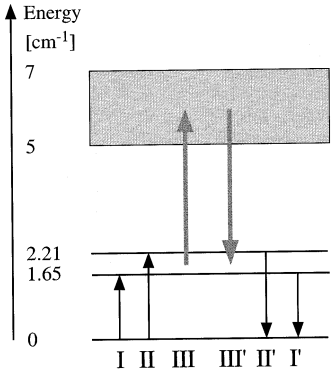


**Figure 7.** Empirical energy level diagram derived from the INS spectra in Figures 4 and 5. The arrows correspond to the observed bands I−III. The unresolved band system III between 3 and 5 cm$^{-1}$ is represented by the gray band.

temperature independent and consists of several unresolved transitions between 3 and 5 cm$^{-1}$. The 7.0 K spectrum exhibits its counterpart labeled III′ as a shoulder on the neutron-energy gain side. In Figure 6, we show INS spectra at an incident neutron wavelength of $\lambda = 4.2$ Å. A broad, unresolved inelastic feature is observed between 10 and 20 cm$^{-1}$. It is predominantly cold and has its counterpart on the neutron-energy gain side at 17 K. As will be shown in section 4.3, we ascribe it to phonon scattering.

From the experimental data presented in Figures 4 and 5, the energy level diagram shown in Figure 7 is derived. The cold transitions I and II are shown as full arrows. The unresolved magnetic intensity between 3 and 5 cm$^{-1}$ is indicated as a gray band. Its virtual temperature independence suggests that it is due to transitions not starting from the lowest level but presumably from those at 1.65 and 2.21 cm$^{-1}$ defined by bands I and II, respectively. In contrast to the energies, determination of exact relative intensities is more difficult. In both the 8.0 and 5.9 Å spectra, the inelastic features are close to the elastic peak, and their intensity may therefore be obscured by quasielastic features. The background of the 8.0 Å spectrum seems to change upon heating from 1.8 to 7.0 K, see Figure 4. The unresolved band III, which is clearly recognized in the 5.9 Å spectrum at 1.8 K, is barely seen in the 8.0 Å spectrum. This suggests that the intensity of weaker bands is not resolved but hidden in the background. We are therefore left with bands I and II, whose intensities were determined by least-squares fitting with two Gaussians and the backgrounds depicted in Figure 4. The result is shown in Table 1. It reveals that bands I and II

**Table 1.** Experimentally Determined Energies, Linewidths (fwhm), and Relative Intensities with Estimated Errors of the INS Bands I and II Derived from the 8.0 Å Spectra for Neutron-Energy Loss[a]

| | energy [cm$^{-1}$] | | | normalized intensity [arb.units] 1.8 K | | 7.0 K | | |
|---|---|---|---|---|---|---|---|---|
| | expt | calcd | fwhm [cm$^{-1}$] | expt | calcd | expt | calcd | assignment |
| I | 1.65 | 1.65 | 0.30 | 1.00(8) | 1.00 | 0.3(1) | 0.33 | |
| Ia | | 1.65 | | | 0.73 | | 0.23 | $\|[0-3]\ ^3/_2\ ^1/_2\rangle \rightarrow \|[1-3]\ ^5/_2\ ^3/_2\rangle$ |
| Ib | | 1.87 | | | 0.27 | | 0.10 | $\|[1,2]\ ^1/_2\ ^1/_2\rangle \rightarrow \|[0-3]\ ^3/_2\ ^3/_2\rangle$ |
| II | 2.21 | 2.21 | 0.25 | 0.90(9) | 0.98 | 0.3(1) | 0.31 | |
| IIa | | 2.21 | | | 0.68 | | 0.20 | $\|[0-3]\ ^3/_2\ ^1/_2\rangle \rightarrow \|[0-3]\ ^3/_2\ ^3/_2\rangle$ |
| IIb | | 2.21 | | | 0.30 | | 0.11 | $\|[1,2]\ ^1/_2\ ^1/_2\rangle \rightarrow \|[1,2]\ ^1/_2\ ^3/_2\rangle$ |

[a] The intensities were normalized to a value of 1.0 for band I at 1.8 K. Calculated energies and intensities of the transitions Ia, Ib and IIa, IIb, using the parameter values $J_{CrNi} = 1.47$ cm$^{-1}$ and $J_{CrCr} = 1.25$ cm$^{-1}$, are given for comparison. The last column gives their assignment in terms of $|[S_{12}]S_{123}S\rangle$ wavefunctions.

essentially have equal relative intensities and temperature dependences. Both I and II do not exhibit a pronounced $Q$ dependence, which we ascribe to the fact that the sample was completely undeuterated and the $Q$ dependence got lost by multiple scattering. A fraction of these processes are incoherent because of the large number of hydrogen atoms in the sample. Thus, the $\vec{k}$ vectors of both the incoming and scattered neutrons and hence the resulting $\vec{Q}$ vector are no longer well defined, which leads to an averaging of the scattered intensity as a function of $Q$.[16]

## 4. Analysis

**4.1. Exchange Coupling Model for $\{Cr_3Ni\}^{5+}$.** According to the exchange coupling scheme in Figure 1b, both nearest-neighbor interactions between each of the $Cr^{3+}$ ions and the central $Ni^{2+}$ ion, and next-nearest neighbor interactions between the $Cr^{3+}$ ions, are considered. On the other hand, intercluster interactions can safely be neglected because the magnetic centers of the clusters are well shielded by the bulky ligands. Because the site symmetry at the $Ni^{2+}$ site in $\{Cr_3Ni\}I_5$ is not exactly trigonal, see section 2.1, there exist two or even three crystallographically inequivalent sites for the $Cr^{3+}$ ions. With reference to Figure 1b, this may result in slightly different exchange parameters between Cr(1)−Ni(4), Cr(2)−Ni(4), and Cr(3)−Ni(4). However, as will be shown from the analysis of the INS data in section 4.3, this effect is negligibly small in $\{Cr_3Ni\}I_5$. Because both $Cr^{3+}$ ($^4A_2$) and $Ni^{2+}$ ($^3A_2$) have orbitally nondegenerate ground states in an octahedral environment, isotropic exchange interactions can be expected. However, the single-ion $S = 1$ state of $Ni^{2+}$ may be considerably split by second-order spin−orbit coupling in zero field.[17] In $[Ni_4(H_2O)(PW_9O_{34})_2]^{10-}$, for example, an axial single-ion anisotropy parameter $D = 4.9$ cm$^{-1}$ was derived from analysis of INS spectra.[18] We parametrize this by an axial zero-field splitting (ZFS) term. For the simplicity of our model, we neglect the ZFS of the single-ion $S = {}^3/_2$ state of $Cr^{3+}$, which usually is very small.[17] Thus, the appropriate effective spin Hamiltonian at zero magnetic field is given by

$$\mathscr{H} = J_{CrNi}(\boldsymbol{S_1}\cdot\boldsymbol{S_4} + \boldsymbol{S_2}\cdot\boldsymbol{S_4} + \boldsymbol{S_3}\cdot\boldsymbol{S_4}) + J_{CrCr}(\boldsymbol{S_1}\cdot\boldsymbol{S_2} + \boldsymbol{S_1}\cdot\boldsymbol{S_3} + \boldsymbol{S_2}\cdot\boldsymbol{S_3}) + D\left[S_{4z}^2 - \frac{1}{3}(S_4(S_4+1))\right] \quad (1)$$

with $S_1 = S_2 = S_3 = {}^3/_2$ for the $Cr^{3+}$ ions and $S_4 = 1$ for the $Ni^{2+}$ ion, respectively. $J_{CrNi}$ and $J_{CrCr}$ are the exchange parameters for the $Cr^{3+}-Ni^{2+}$ and $Cr^{3+}-Cr^{3+}$ interactions, respectively, where positive values correspond to antiferromagnetic interactions. $D$ is the axial ZFS parameter for $Ni^{2+}$.

We use the following coupling scheme:

$$\vec{S}_{12} = \vec{S}_1 + \vec{S}_2,\ \vec{S}_{123} = \vec{S}_{12} + \vec{S}_3,\ \text{and}\ \vec{S} = \vec{S}_{123} + \vec{S}_4 \quad (2)$$

which gives rise to 34 basis functions of the type $|[S_{12}]\ S_{123}\ SM\rangle$. According to Hamiltonian (eq 1), their energies are independent of $S_{12}$, and therefore, they are up to 4-fold degenerate with respect to $S_{12}$. Using the procedures described in refs 19 and 20, we have derived the irreducible representations of all the 34 individual levels in the $C_3$ cluster symmetry, see Table 2. The 4-fold degenerate $|[0-3]\ ^3/_2\ ^1/_2\rangle$ state, for example, consists of three levels that transform as $^2A$, $^2A$, and $^2E$. Adding higher-order terms such as biquadratic exchange in the Hamiltonian (eq 1) would lift these $S_{12}$ degeneracies. However, as will be shown in section 4.3, any such splittings are smaller than our instrumental resolution of 0.25 cm$^{-1}$ in Figure 4. Therefore, we can neglect higher-order exchange terms in $\{Cr_3Ni\}^{5+}$.

The ZFS term in eq 1 mixes the $|[S_{12}]S_{123}SM\rangle$ basis functions, giving rise to functions of the form

$$\psi_n = \sum_M a_n(S_{12}, S_{123}, S, M)|[S_{12}]S_{123}SM\rangle \quad (3)$$

where $a_n(S_{12}, S_{123}, S, M)$ are the eigenvector coefficients obtained by diagonalizing the energy matrix given by the operator in eq 1. The correct wave functions as well as their eigenvalues were calculated using the program ANIMAG,[21] which makes use of a formalism based on the successive use of irreducible tensor operator techniques and is of general validity. Neglecting the ZFS term in eq 1, the $|[S_{12}]S_{123}SM\rangle$

(16) Andres, H. P.; Basler, R.; Güdel, H. U.; Aromi, G.; Christou, G.; Büttner, H.; Rufflé, B. *J. Am. Chem. Soc.* **2000**, *122*, 12469.
(17) Carlin, R. L. *Magnetochemistry*; Springer-Verlag: Berlin, 1986; p 63.
(18) Clemente-Juan, J. M.; Andres, H.; Borrás-Almenar J. J.; Coronado, E.; Güdel, H. U.; Aebersold, M.; Kearly, G.; Büttner, H.; Zolliker, M. *J. Am. Chem. Soc.* **1999**, *121*, 10021.
(19) Griffith, J. S. *Struct. Bonding (Berlin)* **1972**, *10*, 87.
(20) Tsukerblat, B. S.; Belinskii, M. I.; Fainzilberg, V. E. Magnetochemistry and Spectroscopy. In *Soviet Scientific Reviews, B, Chemistry Reviews*; Vol'pin, M. E., Ed.; Harwood Academic Publishers: Amsterdam, 1987; Vol. 9, p 337.
(21) Borrás-Almenar, J. J.; Clemente-Juan, J. M.; Coronado, E.; Tsukerblat, B. S. *Inorg. Chem.* **1999**, *38*, 6081.

**Table 2.** Irreducible Representations of All the 34 Spin States of $\{Cr_3Ni\}^{5+}$ in $C_3$ Symmetry

| $\|[S_{12}]\ S_{123}\ S\rangle$ | irrep | $\|[S_{12}]\ S_{123}\ S\rangle$ | irrep |
|---|---|---|---|
| $\|[3]\ ^9/_2\ ^{11}/_2\rangle$ | $^{12}$A | $\|[1-3]\ ^5/_2\ ^5/_2\rangle$ | $^6$E, $^6$A |
| $\|[2, 3]\ ^7/_2\ ^9/_2\rangle$ | $^{10}$E | $\|[2, 3]\ ^7/_2\ ^5/_2\rangle$ | $^6$E |
| $\|[3]\ ^9/_2\ ^9/_2\rangle$ | $^{10}$A | $\|[1, 2]\ ^1/_2\ ^3/_2\rangle$ | $^4$E |
| $\|[1-3]\ ^5/_2\ ^7/_2\rangle$ | $^8$E, $^8$A | $\|[0-3]\ ^3/_2\ ^3/_2\rangle$ | $^4$E, $^4$A, $^4$A |
| $\|[2, 3]\ ^7/_2\ ^7/_2\rangle$ | $^8$E | $\|[1-3]\ ^5/_2\ ^3/_2\rangle$ | $^4$E, $^4$A |
| $\|[3]^9/_2\ ^7/_2\rangle$ | $^8$A | $\|[1, 2]\ ^1/_2\ ^1/_2\rangle$ | $^2$E |
| $\|[0-3]\ ^3/_2\ ^5/_2\rangle$ | $^6$E, $^6$A, $^6$A | $\|[0-3]\ ^3/_2\ ^1/_2\rangle$ | $^2$E, $^2$A, $^2$A |

basis functions are proper eigenfunctions, and the corresponding eigenvalues are derived in a simple way using the Kambe vector coupling method:[22]

$$E(S_{123}, S) = \frac{J_{\mathrm{CrNi}}}{2}[S(S+1) - S_{123}(S_{123}+1)] + \frac{J_{\mathrm{CrCr}}}{2}[S_{123}(S_{123}+1)] \quad (4)$$

There are in total 14 spin states with total spin quantum numbers ranging from $S = {}^1/_2$ to $^{11}/_2$. Which one of these is the ground state depends critically on the ratio $J_{\mathrm{CrNi}}/J_{\mathrm{CrCr}}$.

In the Hamiltonian (eq 1), we have 3 adjustable parameters, namely $J_{\mathrm{CrNi}}$, $J_{\mathrm{CrCr}}$, and $D$. In the case of an applied magnetic field, the appropriate Zeeman terms with additional $g$ parameters for $Cr^{3+}$ and $Ni^{2+}$ have to be added. Obviously, the magnetic data do not contain enough information for an unambiguous determination of all these parameters. However, they allow us to limit the exchange parameter space, which turned out to be essential for an analysis of the INS data.

**4.2. Rough Estimate of Exchange Parameters from Magnetic Data.** We start with the analysis of the magnetic susceptibility curve of the $\{Cr_3Zn\}I_5$ cluster shown in Figure 2. The product $\chi T$ gradually decreases with temperature from a value of 5.46 cm$^3$ K mol$^{-1}$ at 300 K, corresponding to the spin-only value for three uncoupled $S = {}^3/_2$ spins, to 1.48 cm$^3$ K mol$^{-1}$ at 1.8 K. The experimental data are perfectly reproduced by the parameter values $J_{\mathrm{CrCr}} = 1.12$ cm$^{-1}$ and $g_{\mathrm{Cr}} = 1.97$ using the second term of the Hamiltonian (eq 1) and the appropriate Zeeman term, see Figure 2. The value $J_{\mathrm{CrCr}} = 1.12$ cm$^{-1}$ gives rise to an $S = {}^1/_2$ ground state and is very similar to the value $J_{\mathrm{CrCr}} = 1.06$ cm$^{-1}$ reported for $\{Cr_3Zn\}(ClO_4)_5$.[12]

The magnetic susceptibility curve for $\{Cr_3Ni\}I_5$ shown in Figure 2 starts at a value $\chi T = 6.58$ cm$^3$ K mol$^{-1}$ at 300 K, which agrees with the expected value for three uncoupled spins $S = {}^3/_2$ with $g = 1.97$, the value found in $\{Cr_3Zn\}(ClO_4)_5$, and one spin $S = 1$ with $g = 2.26$. $\chi T$ decreases with temperature down to 2.08 cm$^3$ K mol$^{-1}$ at 1.8 K, with a clear tendency toward smaller values at lower temperature. This is indicative of an $S = {}^1/_2$ ground state, requiring both $J_{\mathrm{CrNi}}$ and $J_{\mathrm{CrCr}}$ to be antiferromagnetic. The decrease of $\chi T$ below 50 K is very steep, from which we estimate a total exchange splitting of the manifold of all the spin states in the order of 20−30 cm$^{-1}$.

The magnetization in Figure 3 increases with the field up to $M/N\mu_{\mathrm{B}} = 6$ at 5 T and 1.8 K, where it is still not saturated. Furthermore, the magnetization data for different fields do not superimpose, which reveals the existence of excited states at energies in the order of the Zeeman splitting. The highest magnetization value of $M/N\mu_{\mathrm{B}} = 6$ measured at 1.8 K and 5 T clearly indicates the participation of $M = -{}^5/_2$ or $-{}^7/_2$ Zeeman components. If only the $S = {}^1/_2$ and $S = {}^3/_2$ cluster states were populated, the saturation magnetizations would be $M/N\mu_{\mathrm{B}} = g_S/2 \approx 1$ and $M/N\mu_{\mathrm{B}} = 3g_S/2 \approx 3$, respectively, where $g_S$ are the $g$ values of the respective cluster spin states. We conclude that within a few wavenumbers from the $S = {}^1/_2$ ground state there are excited states with $S$ values of $^5/_2$ or higher. From the arithmetic of eq 4, it follows that this can only be achieved if both $J_{\mathrm{CrNi}}$ and $J_{\mathrm{CrCr}}$ are positive and on the order of 1−2 cm$^{-1}$. A more accurate determination of the exchange parameters from the magnetic data is not possible. But having successfully narrowed the possible exchange parameter range, we are now in a position to quantitatively analyze the INS spectra.

**4.3. Analysis of the INS Spectra.** With the restrictions derived from the magnetic data, we can now tentatively assign the energy levels derived from INS in Figure 7: The ground state is $S = {}^1/_2$, the two levels at 1.65 and 2.21 cm$^{-1}$ are likely $S = {}^3/_2$ levels, and the band between 4.5 and 6 cm$^{-1}$ must be due to transitions to $S = {}^5/_2$ and/or $S = {}^7/_2$ levels. The relative INS intensities of bands I and II is the key to a more detailed analysis. Therefore, we compute relative INS intensities and compare them with experiment. For a transition between the levels $|\psi_n\rangle$ and $|\psi_m\rangle$, the intensity is given by the partial differential neutron cross section:[23]

$$\frac{\mathrm{d}^2\sigma}{\mathrm{d}\Omega \mathrm{d}E} = \mathcal{O}(Q, T) \sum_{\alpha,\beta}\left\{\delta_{\alpha,\beta} - \frac{Q_\alpha Q_\beta}{Q^2}\right\} \times \sum_{i,j}\{g_i F_i(Q)\}\{g_j F_j(Q)\} \exp(i\vec{Q}(\vec{R}_i - \vec{R}_j)) \times \langle\psi_n|\hat{S}_i^\alpha|\psi_m\rangle\langle\psi_m|\hat{S}_j^\beta|\psi_n\rangle \quad (5)$$

where

$$\mathcal{O}(Q, T) = \frac{1N}{4Z}\left\{\frac{\gamma e^2}{m_e c^2}\right\}\frac{k'}{k} \exp(-2W(Q, T)) \times \exp\left\{\frac{-E_{\psi n}}{k_{\mathrm{B}}T}\right\}\delta(\hbar\omega + E_{\psi n} + E_{\psi m})$$

In eq 5, $k$ and $k'$ are the wavenumbers of the incoming and scattered neutrons, $\vec{Q}$ is the scattering vector, $\exp(-2W(Q, T))$ is the Debye−Waller factor, $g_i$ is the Landé factor, $F_i(Q)$ is the magnetic form factor, $\vec{R}_i$ is the space vector of the $i$th metal ion,[24] $\gamma$ is the gyromagnetic constant of the neutron, and $\alpha$ and $\beta$ stand for the spatial coordinates $x$, $y$, $z$. The remaining symbols have their usual meaning. The cross section was calculated with the program ANIMAG using the formalism described in ref 21. Because our experiments were performed on a powdered sample with random orientation of the cluster with respect to the scattering vector $\vec{Q}$,

(22) Boudreaux, E. A.; Mulay, E. N. *Theory and Applications of Molecular Paramagnetism*; Wiley-Interscience: New York, 1976; p 377.

(23) Marshall, W.; Lovesey, S. W. *Theory of thermal neutron scattering*; Claredon Press: Oxford, 1971.

(24) Because of the lack of structural data for $\{Cr_3Ni\}I_5$, the space vectors are based on the crystal structure of $\{Cr_3Ni\}(ClO_4)_5$ from ref. 12.

the cross section had to be summed over the $\vec{Q}$ space. For INS transitions between the basis functions, the following selection rules apply:

$$\Delta S_{12} = 0, \pm 1$$

$$\Delta S_{123} = 0, \pm 1$$

$$\Delta S = 0, \pm 1$$

$$\Delta M = 0, \pm 1 \qquad (6)$$

With reference to Figures 4 and 5, the INS spectra in the energy range between 0 and 5 $cm^{-1}$ are governed by the intense, cold bands I and II.

An $S = {}^1/_2$ cluster ground state is firmly established from the magnetic measurements. According to the selection rule $\Delta S = 0, \pm 1$ in eq 6, INS transitions to $S = {}^3/_2$ states are allowed, and we assign the bands I and II to $S = {}^1/_2 \rightarrow S = {}^3/_2$ transitions. Using the parameter values

$$J_{CrNi} = 1.47\ cm^{-1} \qquad J_{CrCr} = 1.25\ cm^{-1} \qquad (7)$$

the experimentally determined transition energies of 1.65 and 2.21 $cm^{-1}$ for bands I and II, respectively, as well as their intensities, are well reproduced, see Table 1. This is also shown in Figure 4, where the calculated spectra are plotted as solid lines.

In Figure 8, we show the complete energy level diagram calculated with the exchange parameter values from eq 7. Because there is no anisotropy (vide infra), the levels are denoted with their basis functions $|[S_{12}]S_{123}S\rangle$. Full arrows represent the INS transitions observed in Figures 4 and 5. Both bands I and II are each a superposition of two transitions, see Table 1 and Figure 8. For band I, these transitions are $|[0-3]\ {}^3/_2\ {}^1/_2\rangle \rightarrow |[1-3]\ {}^5/_2\ {}^3/_2\rangle$ and $|[1,2]\ {}^1/_2\ {}^1/_2\rangle \rightarrow |[0-3]\ {}^3/_2\ {}^3/_2\rangle$ labeled as Ia and Ib, respectively. Band II consists of the transitions $|[0-3]\ {}^3/_2\ {}^1/_2\rangle \rightarrow |[0-3]\ {}^3/_2\ {}^3/_2\rangle$ and $|[1,2]\ {}^1/_2\ {}^1/_2\rangle \rightarrow |[1,2]\ {}^1/_2\ {}^3/_2\rangle$ denoted as IIa and IIb, respectively. Transition Ia occurs at an energy of 1.65 $cm^{-1}$ and is about 3 times more intense than transition Ib at 1.87 $cm^{-1}$, see Table 1. Because Ia dominates, the experimentally observed band I peaks at the same energy, but the different energies of Ia and Ib lead to a significant broadening and an asymmetric shape of band I, see Figure 4 and Table 1. Its line width (fwhm) of 0.30 $cm^{-1}$ is substantially larger than the instrumental resolution. The latter has a value of 0.22 $cm^{-1}$ at the elastic peak position and slightly increases with the neutron energy loss. In contrast, the two transitions IIa and IIb occur at exactly the same energy value of 2.21 $cm^{-1}$. Therefore, band II is sharper; its line width of 0.25 $cm^{-1}$ essentially corresponds to the instrumental resolution. Transitions between $|[S_{12}]S_{123}S\rangle$ states with the same total spin quantum number $S$ are shown on the right of Figure 8. They occur at energies below 0.7 $cm^{-1}$ and may therefore form part of the shoulder near the elastic peak on the energy gain side of the 8.0 Å spectra in Figure 4. Band III is a superposition of several unresolved $S = {}^3/_2 \rightarrow S = {}^5/_2$ transitions. $S = {}^5/_2 \rightarrow S = {}^7/_2$ and $S = {}^7/_2 \rightarrow S = {}^9/_2$ transitions shown as dashed arrows in Figure 8 arise at 7.0 K, but they

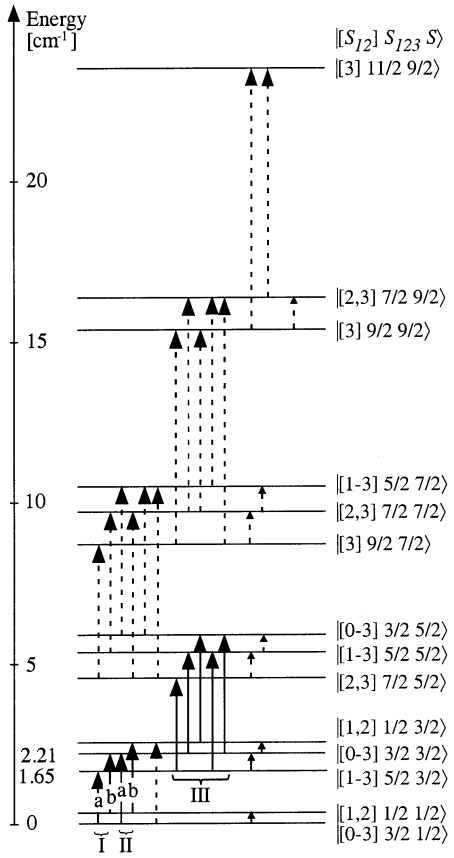


**Figure 8.** Complete energy level diagram of the $\{Cr_3Ni\}I_5$ cluster calculated with the parameter values $J_{CrNi} = 1.47\ cm^{-1}$ and $J_{CrCr} = 1.25\ cm^{-1}$ derived from the INS spectra. Experimentally observed INS transitions are shown as solid arrows. Dashed arrows indicate unresolved transitions at 7.0 K. The levels are denoted as $|[S_{12}]S_{123}S\rangle$.

are not resolved and simply add to the background in the experimental spectra above 4 $cm^{-1}$. The total splitting of all spin states due to exchange interactions is 23.4 $cm^{-1}$.

The experimentally observed selective intensity distribution and the narrow width of the bands in Figure 4 are very strong indications that deviations from the trigonal cluster symmetry are negligibly small, because otherwise the energies would depend on $S_{12}$ (see eq 2). This would result in additional splittings of spin states, giving rise to a multitude of observable transitions with comparable intensity. Furthermore, these observations clearly indicate that any interactions such as local anisotropy and biquadratic exchange (see section 4.1) that lead to further splittings of spin states are negligibly small. As EPR spectra of $\{Cr_3Ni\}I_5$ exhibited only broad, uncharacteristic features, we are left with the information from the INS spectra that allows for setting upper limits to the magnitudes of these interactions. Thus, the ZFS of the $S = {}^3/_2$ states has to be smaller than 0.25 $cm^{-1}$, the observed width of band II in Figure 4. This value translates to a ZFS parameter of $|D| \leq 1\ cm^{-1}$ in eq 1. Similarly, the fine splittings due to biquadratic exchange interactions have to be smaller than 0.25 $cm^{-1}$. We have performed test calculations with biquadratic terms $\mathscr{H}_{BQ} = -j_{CrNi}[(\boldsymbol{S_1}\cdot\boldsymbol{S_4})^2 + (\boldsymbol{S_2}\cdot\boldsymbol{S_4})^2 + (\boldsymbol{S_3}\cdot\boldsymbol{S_4})^2] - j_{CrCr}[(\boldsymbol{S_1}\cdot\boldsymbol{S_2})^2 + (\boldsymbol{S_1}\cdot\boldsymbol{S_3})^2 + (\boldsymbol{S_2}\cdot\boldsymbol{S_3})^2]$ added to the Hamiltonian (eq 1). The largest parameter values that do not significantly broaden bands I and II are $j_{CrNi} =$

+0.01 cm$^{-1}$ and $j_{CrCr} = -0.01$ cm$^{-1}$. They are less than 1% of $J_{CrNi}$ and $J_{CrCr}$ in magnitude. The ratio $j/J$ is typically on the order of 1/100.[25] In conclusion, because splittings or line broadenings due to local anisotropy or biquadratic exchange interactions are not observed in the INS spectra, we can safely neglect these interactions in our analysis.

According to Figure 8, there are no allowed transitions in the energy range between 10 and 20 cm$^{-1}$ that could explain the broad inelastic band in Figure 6. Cold magnetic transitions in this energy range could only get intensity upon a strong mixing of the $|[S_{12}]S_{123}SM_S\rangle$ basis functions due to a large ZFS, and this we have ruled out on the basis of the 8.0 Å spectra, vide supra. Therefore, the origin of the broad band in Figure 6 has to be nonmagnetic. We ascribe it to phonon modes. The density of vibrational states with a substantial hydrogen contribution appears to be large enough in this energy range to lead to observable phonon excitations. The fact that we used a nondeuterated sample in this study may also lead to the relatively high background in the 8.0 and 5.9 Å spectra of Figures 4 and 5, respectively.

With the exchange parameter values in eq 7 derived from the INS spectra and the $g$ values as adjustable parameters, we can now calculate the magnetic susceptibility and magnetization curves using the numerical procedure developed in ref 21. For both $Cr^{3+}$ and $Ni^{2+}$, we use isotropic $g$ values. $g_{Cr}$ was fixed to 1.97, the value found for {$Cr_3Zn$}-$I_5$, see section 4.1. $g_{Ni}$ was then varied to reproduce the $\chi T$ value at 300 K, obtaining $g_{Ni} = 2.26$, a reasonable value for $Ni^{2+}$. With these parameters, the susceptibility curve for {$Cr_3$-Ni}$I_5$ is generally well reproduced, see the full line through the data in Figure 2. The magnetization curves calculated with the same parameter set are shown as solid lines in Figure 3. The experimentally observed dependence of the magnetization on the applied field for a given $H/T$ ratio is fairly well reproduced. This reflects the small energy spacings between the cluster spin states, see Figure 8, which are smaller than the Zeeman energies. However, the agreement between the observed and calculated magnetization values becomes rather poor at high $H/T$ ratios. Test calculations have shown that using a small ZFS parameter of $|D| = 1$ cm$^{-1}$, the upper limit derived from the INS spectra, as well as including parameters for biquadratic exchange, does not significantly alter the magnetization curves. The same is true for a small geometric distortion from trigonal symmetry. Thus, neither this nor the neglect of ZFS and higher-order exchange terms accounts for the observed deviations. A possible reason for them may be a second-order Zeeman effect. However, a careful comparison of the experimental and calculated curves in Figure 3 reveals that the magnetization is slightly overestimated by the calculation just above about 6 K. Therefore, at least part of the deviations have to be due to an impurity in the sample, and from the amount of overestimation, we estimate an impurity amount on the order of 4−5%. This value would affect neither the results of the chemical analysis and powder X-ray data, see section 2.1, nor the INS spectra. Such a small impurity may also be responsible for the slightly higher experimental $\chi T$ curve compared to the calculated one below 5 K, see Figure 2.

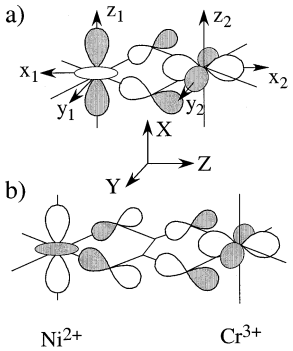


**Figure 9.** Schematic representation of the relevant antiferromagnetic orbital exchange pathway: (a) in the $Cr(OH)_2Ni$ core of {$Cr_3Ni$}$I_5$ and (b) in the Cr(ox)Ni core of {Cr[(ox)NiL]$_3$}$(ClO_4)_3$ (L = 5,7,7,12,14,14-hexamethyl-1,4,8,11-tetraazacyclotetradecane).[1] $x_i$, $y_i$, $z_i$ ($i$ = 1,2) and $X$, $Y$, $Z$ denote the local and pair coordinate systems, respectively. Only the half-filled orbitals on $Cr^{3+}$ and $Ni^{2+}$ transforming as $a_1$ in the approximate $C_{2v}$ symmetry of the Cr−Ni pair are shown, together with the relevant p orbitals on the oxygen ligator atoms. The orbitals on the carbon atoms of the oxalate are omitted for clarity.

Nevertheless, with our simple isotropic exchange model and the parameter values $J_{CrNi} = 1.47$ cm$^{-1}$ and $J_{CrCr} = 1.25$ cm$^{-1}$, the experimental data are generally well reproduced, and we can therefore be confident that both the model and the parameter values are physically meaningful.

## 5. Discussion

Our analysis provided three major results: (i) the exchange parameters $J_{CrCr}$ and $J_{CrNi}$ are both antiferromagnetic, (ii) they are of similar magnitude, and (iii) single-ion anisotropies are negligibly small with an upper value for the ZFS parameter on $Ni^{2+}$ of $|D| \leq 1$ cm$^{-1}$. The second point is astonishing at first sight, because the $Cr^{3+}-Ni^{2+}$ interaction occurs between nearest neighbors, whereas $Cr^{3+}-Cr^{3+}$ is a next-nearest neighbor interaction. The small antiferromagnetic value of the $Cr^{3+}-Ni^{2+}$ interaction can be rationalized on the basis of the relevant orbital exchange parameters following the argumentation in refs 26 and 27. The exchange parameter $J_{CrNi}$ is composed of several orbital contributions which can either be positive or negative. Only orbital parameters corresponding to overlapping, half-filled orbitals can provide positive contributions to $J_{CrNi}$, and the better the orbital overlap, the larger the resulting antiferromagnetic contribution is. The local symmetry of the $Cr(OH)_2Ni$ bridging geometry is approximately $C_{2v}$ with the pair coordinate system $X$, $Y$, $Z$ shown in Figure 9.

The half-filled orbitals on the $Ni^{2+}$ ($d^8$) are denoted as $d_{z^2}$ and $d_{xy}$ and transform as $a_1$ and $b_1$ in $C_{2v}$, respectively. The half-filled orbitals on $Cr^{3+}$ ($d^3$) are $d_{x^2-y^2}$, $d_{xz}$, and $d_{yz}$, transforming as $a_1$, $b_2$, and $a_2$, respectively.[28] $J_{CrNi}$ can then be expressed as the sum of 6 orbital parameters $J_{ij}$ as follows:

(25) McCarthy, P. J.; Güdel, H. U. *Coord. Chem. Rev.* **1988**, *88*, 69.

(26) Ginsberg, A. P. *Inorg. Chim. Acta, Rev.* **1971**, *5*, 45.

(27) Kahn, O. *Molecular Magnetism*; VCH Publishers: New York, 1993; p 192.

(28) Note that the orbitals are denoted in the local $x_i$, $y_i$, $z_i$ ($i$ = 1, 2) coordinate systems, while their symmetry representations refer to the pair $X$, $Y$, $Z$ axes, see Figure 9.

$$J_{CrNi} = \frac{1}{6}[J_{a_1a_1} + J_{a_1b_1} + J_{b_2a_1} + J_{b_2b_1} + J_{a_2a_1} + J_{a_2b_1}] \quad (8)$$

Except for $J_{a_1a_1}$, all the $J_{ij}$'s in eq 7 involve orbitals which are orthogonal to each other by symmetry and are thus necessarily negative. Thus, $J_{a_1a_1}$ corresponds to the only antiferromagnetic exchange pathway in the $Cr^{3+}-Ni^{2+}$ pair, for which the relevant orbitals are shown in Figure 9a for the title complex. The $d_{x^2-y^2}$ orbital on $Cr^{3+}$ has a $\pi$-type overlap with p orbitals centered on the oxygen atoms. These p orbitals, in turn, undergo a $\sigma$-type interaction with the $d_{z^2}$ orbital on the $Ni^{2+}$. Thus, the antiferromagnetic $J_{CrNi}$ value of 1.47 $cm^{-1}$ is the result of a fine balance between the antiferromagnetic and ferromagnetic contributions.

The positive value for $J_{CrNi}$ is in contrast to the oxalato-bridged complexes, in which the net $Cr^{3+}-Ni^{2+}$ interactions are ferromagnetic. For the trigonal $[CrNi_3]$ cluster $\{Cr[(ox)NiL]_3\}(ClO_4)_3$ (L = 5,7,7,12,14,14-hexamethyl-1,4,8,11-tetraazacyclotetradecane), a value of $J_{CrNi} = -5.3$ $cm^{-1}$ has been reported.[1] Obviously, the balance is altered when going from di-$\mu$-hydroxo to oxalato-bridged complexes. The situation for the latter is depicted in Figure 9b. We note that the situation on the metals remains unchanged compared to the di-$\mu$-hydroxo-bridged complex, except for the different phase of the $d_{z^2}$ orbital. However, the partial delocalization now has to occur over 3 ligand atoms instead of one, leading to a substantial weakening of the antiferromagnetic pathway. The resulting $J_{a_1a_1}$ is, therefore, not large enough to compete against the numerous negative $J_{ij}$, giving rise to a negative value for $J_{CrNi}$.

In conclusion, the title compound is an illustrative example of the complications which arise in the interpretation of the magnetic properties of higher-nuclear complexes in which different interactions of similar magnitude are competing. We can safely assume that the exchange coupling of the $\{Cr_3Ni\}^{5+}$ cluster is the same in the perchlorate and iodide salts. For $\{Cr_3Ni\}(ClO_4)_5$, exchange parameter values of $J_{CrNi} = 4.87$ $cm^{-1}$ and $J_{CrCr} = 1.06$ $cm^{-1}$ were derived in ref 12 from a susceptibility curve measured down to 5 K only, where $\chi T$ is still $\approx 4$ $cm^3$ K $mol^{-1}$. Above 5 K, however, the curve is not very informative, which led to these obviously erroneous parameter values. They correspond to an $S = {}^7/_2$ ground state, which could as well be achieved with a negative $J_{CrNi}$. Therefore, not even the sign of $J_{CrNi}$ can unambiguously be determined from magnetic susceptibility down to 5 K. In the present study, the overall antiferromagnetic nature of the exchange in $\{Cr_3Ni\}^{5+}$ could be derived from magnetic susceptibility down to 1.8 K. However, the crucial information comes from INS, which directly accesses the lowest-energy spin states. The high-resolution 8.0 Å INS spectra turned out to be the key to deriving the exchange and anisotropy parameters.

**Acknowledgment.** This work was financially supported by the Swiss National Science Foundation and the European Science Foundation.

IC0111031